Yokohama Publishers
ISSN 1349-8169 ONLINE JOURNAL

Pacific Journal of Optimization
Vol. 11, No. 4, pp. 763–790, October 2015

ON THE CONTROLLABILITY OF DIFFUSION PROCESSES ON THE SURFACE OF A TORUS: A COMPUTATIONAL APPROACH

D. Assaely León-Velasco, Roland Glowinski and L. Héctor Juárez-Valencia

Abstract: The main goal of this article is to study computationally the controllability of a diffusion process on the surface of a torus in $\mathbb{R}^3$. To achieve this goal, we employ a methodology combining finite differences for the time discretization, finite elements for the space approximation, and a conjugate gradient algorithm for the iterative solution of the discrete control problems. The results of numerical experiments, obtained using the above methodology, will be presented. Furthermore, the null-controllability properties of the diffusion model under consideration will be also studied computationally.

Key words: *Laplace-Beltrami operator, approximate controllability, null-controllability, diffusion equation, surface of a torus, conjugate gradien, finite element*

Mathematics Subject Classification: *49K20, 58E25, 65K10, 65M60, 93B05, 93C20*

1 Introduction

Many physico–chemical phenomena modeled by partial differential equations take place on the surface of planet Earth; it makes sense therefore to attempt controlling some of them (pollution for example). This evidence leads naturally to control and controllability problems for surfaces of $\mathbb{R}^3$, spheres in particular. Looking at the literature shows that, for example, the control of diffusion processes on surfaces of $\mathbb{R}^3$ has not attracted much attention, yet, despite the fact that such problems have potentially many applications. Actually, the origin of this article is the null–controllability results for the heat equation proved in [9], not only for bounded domains of $\mathbb{R}^d$, but also for Riemannian manifolds, the usual Laplace operator being replaced then by the Beltrami Laplacian. One of our goals in this article is to compute the control of minimal $\mathcal{L}^2$–norm realizing the null–controllability at a given time T. This problem being more complicated than what it looks like (as shown in [12] for example), we decided to approximate it via a sequence of penalized problems, which are relatively easy to solve numerically, by variants of the methods discussed in [2] for the usual heat equation. Albeit computational null–controllability was our driver, we decided to take advantage of the developed methodology to, first, investigate computationally the solution of controllability problems where the target function is different from zero, a much more demanding situation since, in general, diffusion processes are not exactly controllable. The first surfaces of $\mathbb{R}^3$ we decided to consider are the surfaces of circular toruses, for the simple reason that they are easier to parameterize and triangulate than spherical ones which are next in our research

program (preliminary results, to be reported elsewhere, show that the methods discussed in this article extend easily to the solution of controllability problems for diffusion phenomena on spheres of $\mathbb{R}^3$, once a triangular facets based polyhedral approximation of the sphere is available). Actually, toroid shape structures occur in Science and Industry (Tokomak machines for example), but they are clearly less common than spherical ones.

2 Model Problem

2.1 Generalities

As mentioned in Section 1, our goal in this article is to discuss the numerical solution of a controllability problem associated with a diffusion process taking place on the surface Σ of a torus of $\mathbb{R}^3$. The torus and the parameterization of Σ have been visualized in Figure 1, where R (resp., r) is the major (resp., minor) radius. Figure 1 shows also the two angles θ and ϕ used to parameterize Σ.

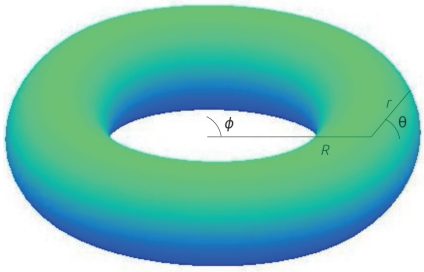

Figure 1: A torus and its surface

Let ω be an open subset of Σ (not necessarily connected). The first problem to be considered is an exact controllability one, namely:

Find $v \in \mathcal{L}^2(\omega \times (0,T))$ such that the solution y of the following parabolic initial value problem

$$\begin{cases} \displaystyle\int_\Sigma \frac{\partial y}{\partial t}(t) z \, d\Sigma + \mu \int_\Sigma \nabla_\Sigma y(t) \cdot \nabla_\Sigma z \, d\Sigma = \int_\omega v(t) z \, d\Sigma, \ \ \forall z \in \mathcal{H}^1(\Sigma), \ \text{ a.e. on } (0,T), \\ y(0) = y_0, \end{cases} \tag{2.1}$$

verifies

$$y(T) = y_T, \tag{2.2}$$

where: (i) ∇_Σ is the *tangential gradient* on Σ. (ii) $d\Sigma$ is the infinitesimal surface measure. (iii) $\mathcal{H}^1(\Sigma) = \left\{ z \,|\, z \in \mathcal{L}^2(\Sigma), \ \int_\Sigma |\nabla_\Sigma z|^2 \, d\Sigma < +\infty \right\}$. (iv) $\mathbf{a} \cdot \mathbf{b} = \sum_{i=1}^3 a_i \, b_i$, $\forall \ \mathbf{a} = (a_i)_{i=1}^3$, $\mathbf{b} = (b_i)_{i=1}^3$. (v) y_0, $y_T \in \mathcal{L}^2(\Sigma)$, and $\mu (> 0)$ is a diffusion coefficient. (vi) $\varphi(t)$ denotes the function $x \longrightarrow \varphi(x,t)$ from Σ (or ω) into $\mathbb{R}$.

The above exact controllability problem has no solution, in general. However, we have *approximate controllability* since the set $\{y(T; v)\}_{v \in \mathcal{L}^2(\omega \times (0,T))}$ is *dense* in $\mathcal{L}^2(\Sigma)$ (see the Chapter 1 of [7] for related results). We will take advantage of the above density results

to define, below, an approximately controllable variant of the above exact controllability problem.

Remark 2.1. Suppose that $y_{_T} = 0$; it follows then from [9] that, $\forall\, y_0 \in \mathcal{L}^2(\Sigma)$, there exists a control $v \in \mathcal{L}^2(\omega)$, such that the solution of the initial value problem (2.1) verifies $y(T) = 0$. This property is known as the *null-controllability property* and holds for sufficiently smooth surfaces of $\mathbb{R}^d$ (and bounded planar domains). We will return on the null-controllability property in Section 6.2.

Remark 2.2. The elliptic operator associated with equation (2.1) is clearly $(-1)\mu$ times the *Laplace–Beltrami operator*.

2.2 Formulation of an Approximate Controllability Problem

Taking advantage of the density results mentioned in Section 2.1, we approximate the exact controllability problem introduced above by the following one (of the *approximation by penalty* type):

$$\begin{cases} u_k \in \mathscr{U}, \\ J_k(u_k) \leq J_k(v),\ \forall v \in \mathscr{U}, \end{cases} \tag{2.3}$$

where $\mathscr{U} = \mathcal{L}^2(\omega \times (0,\, T))$, and the cost functional $J_k : \mathscr{U} \to \mathbb{R}$ is defined by

$$J_k(v) = \frac{1}{2} \int_{\omega \times (0,\, T)} |v|^2 \, d\Sigma \, dt \, + \frac{k}{2} \int_{\Sigma} |y(T) - y_{_T}|^2 \, d\Sigma, \tag{2.4}$$

with $k > 0$, and the function y obtained from the control v via the solution of the initial value problem (2.1). It follows from, e.g., [7] that the approximate controllability problem (2.3) has a unique solution, characterized by

$$DJ_k(u_k) = 0, \tag{2.5}$$

where $DJ_k(u_k)$ is the differential of J_k at u_k. The solution of (2.5) by a conjugate gradient algorithm operating in $\mathscr{U}$ will be discussed in Section 4, but before we will address the computation of $DJ_k(v)$, $\forall v \in \mathscr{U}$, a most important issue, indeed.

Remark 2.3. Using results from [7], one can show that if one denotes by y_k the solution of (2.1) associated with u_k, then

$$\lim_{k \to +\infty} y_k(T) = y_{_T} \ \text{ in } \ \mathcal{L}^2(\Sigma),$$

justifying thus taking (2.3) as approximate controllability problem. On the other hand, unless the exact controllability property holds for the target function $y_{_T}$ under consideration, we have

$$\lim_{k \to +\infty} ||u_k||_{\mathcal{L}^2(\omega \times (0,\, T))} = +\infty.$$

A related result is provided by the following,

Theorem 2.4. *Suppose that the exact controllability property holds for the target function $y_{_T}$. We have then*

$$\lim_{k \to +\infty} u_k = u \ \textit{in} \ \mathcal{L}^2(\omega \times (0,\, T)), \tag{2.6}$$

where, in (2.6), u is the control of minimal norm in $\mathcal{L}^2(\omega \times (0,\, T))$, realizing the exact controllability.

Proof. We will sketch the proof (rather classical) of this most important result. Assuming that it is non–empty, the set of the control functions v, leading to exact controllability, is a closed convex subset of $\mathscr{U}$, implying the uniqueness of the control of minimal norm in $\mathscr{U}$ realizing the above exact controllability property; we will denote this control by u. Taking $v = u$ in (2.3) we obtain

$$\int_{\omega\times(0,\,T)} |u_k|^2\, d\Sigma\, dt + k\int_{\Sigma} |y_k(T) - y_{_T}|^2\, d\Sigma \leq \int_{\omega\times(0,\,T)} |u|^2\, d\Sigma\, dt,\ \forall k > 0. \tag{2.7}$$

Relation (2.7) implies

$$\int_{\omega\times(0,\,T)} |u_k|^2\, d\Sigma\, dt \leq \int_{\omega\times(0,\,T)} |u|^2\, d\Sigma\, dt,\ \forall k > 0 \tag{2.8}$$

and

$$\int_{\Sigma} |y_k(T) - y_{_T}|^2\, d\Sigma \leq k^{-1}\int_{\omega\times(0,\,T)} |u|^2\, d\Sigma\, dt,\ \forall k > 0. \tag{2.9}$$

If follows then from (2.9) that

$$\lim_{k\to+\infty}\int_{\Sigma} |y_k(T) - y_{_T}|^2\, d\Sigma = 0. \tag{2.10}$$

On the other hand, since in the Hilbert space $\mathscr{U}$ the closed ball centered at 0 and of radius $\sqrt{\int_{\omega\times(0,\,T)} |u|^2\, d\Sigma\, dt}$ is weakly compact, it follows from (2.8) that one can extract from $\{u_k\}_{k>0}$ a subsequence — still denoted by $\{u_k\}_{k>0}$ — converging weakly in $\mathscr{U}$ to u^* verifying

$$\int_{\omega\times(0,\,T)} |u^*|^2\, d\Sigma\, dt \leq \int_{\omega\times(0,\,T)} |u|^2\, d\Sigma\, dt. \tag{2.11}$$

From the weak lower semi–continuity of the (convex) function $v \to \int_{\omega\times(0,\,T)} |v|^2\, d\Sigma\, dt$ it follows from (2.8) and (2.11) that

$$\begin{aligned}\int_{\omega\times(0,\,T)} |u^*|^2\, d\Sigma\, dt &\leq \liminf_{k\to+\infty}\int_{\omega\times(0,\,T)} |u_k|^2\, d\Sigma\, dt\\ &\leq \limsup_{k\to+\infty}\int_{\omega\times(0,\,T)} |u_k|^2\, d\Sigma\, dt\\ &\leq \int_{\omega\times(0,\,T)} |u|^2\, d\Sigma\, dt.\end{aligned} \tag{2.12}$$

Using close variants of those techniques developed in [10] for the control of linear parabolic equations we can show that the weak convergence of $\{u_k\}_k$ to u^* implies, in the space

$$W(0,\,T) = \left\{ z \,|\, z \in \mathcal{L}^2(0,\,T;\,\mathcal{H}^1(\Sigma)),\ \frac{\partial z}{\partial t} \in \mathcal{L}^2(0,\,T;\,\mathcal{H}^{-1}(\Sigma)) \right\},$$

the weak convergence of $\{y_k\}_k$ to the function y^*, the unique solution of (2.1) associated with $v = u^*$ (above, $\mathcal{H}^{-1}(\Sigma)$ is the dual space of $\mathcal{H}^1(\Sigma)$). The above convergence result implies—among other properties—that

$$\lim_{k\to+\infty} y_k(T) = y^*(T) \ \text{ weakly in } \mathcal{L}^2(\Sigma). \tag{2.13}$$

Combining the convergence results (2.10), and (2.13) we can easily show that

$$y^*(T) = y_{_T}. \tag{2.14}$$

Relation (2.14) shows that u^* belong to the set of these control functions realizing exact controllability; it follows then from (2.11) and (2.12) that $u^* = u$ and that the whole family $\{u_k\}_{k>0}$ converges (strongly) to u in $\mathscr{U} = \mathcal{L}^2(\omega \times (0,\, T))$. □

Assuming that $y_{_T} = 0$, the above result justifies using the penalty approach to approximate the control function of minimal norm in $\mathscr{U}$ realizing null–controllability.

3 Computation of $DJ_k(v)$. Optimality Conditions

3.1 On the Computation of $DJ_k(v)$

Let $\delta v \in \mathscr{U}$ be a perturbation of $v \in \mathscr{U}$; we have then, with obvious notation,

$$\delta J_k(v) \,=\, \int_{\omega\times(0,\,T)} v\delta v\, d\Sigma\, dt \,+\, k\int_{\Sigma} (y(T) - y_{_T})\, \delta y(T)\, d\Sigma, \tag{3.1}$$

with δy the solution of the following initial value problem (obtained by perturbation of (2.1)–(2.2)):

$$\begin{cases} \displaystyle\int_{\Sigma} \frac{\partial \delta y}{\partial t}(t)\, z\, d\Sigma \,+\, \mu \int_{\Sigma} \nabla_{_\Sigma}\delta y(t)\cdot\nabla_{_\Sigma} z\, d\Sigma \,=\, \int_{\omega} \delta v(t)\, z\, d\Sigma,\ \ \forall z \in \mathcal{H}^1(\Sigma),\ \text{a.e. on } (0,\, T), \\ \delta y(0) = 0. \end{cases} \tag{3.2}$$

Consider now p, a function of x, t (and θ, ϕ, t), verifying $p(t) \in \mathcal{H}^1(\Sigma)$, $\forall t \in (0,\, T)$, and smooth enough as a function of t to authorize integration by parts with respect to t; taking $z = p(t)$ in (3.2), we obtain:

$$\int_{\Sigma\times(0,\,T)} \frac{\partial \delta y}{\partial t}(t)\, p(t)\, d\Sigma\, dt \,+\, \mu \int_{\Sigma\times(0,\,T)} \nabla_{_\Sigma}\delta y(t)\cdot\nabla_{_\Sigma} p(t)\, d\Sigma\, dt \,=\, \int_{\omega\times(0,\,T)} \delta v(t)\, p(t)\, d\Sigma\, dt. \tag{3.3}$$

It follows from (3.3), after time integration by parts, and taking into account the relation $\delta y(0) = 0$, that

$$\int_{\Sigma} p(T)\delta y(T)\, d\Sigma \,-\, \int_{\Sigma\times(0,\,T)} \frac{\partial p}{\partial t}(t)\, \delta y(t)\, d\Sigma\, dt \,+\, \mu \int_{\Sigma\times(0,\,T)} \nabla_{_\Sigma} p(t)\cdot\nabla_{_\Sigma}\delta y(t)\, d\Sigma\, dt \\ = \int_{\omega\times(0,\,T)} p(t)\, \delta v(t)\, d\Sigma\, dt. \tag{3.4}$$

Suppose that p is solution to the *backward in time* initial value problem (the *adjoint* or *co-state equation*):

$$\begin{cases} -\displaystyle\int_{\Sigma} \frac{\partial p}{\partial t}(t)\, z\, d\Sigma \,+\, \mu \int_{\Sigma} \nabla_{_\Sigma} p(t)\cdot\nabla_{_\Sigma} z\, d\Sigma \,=\, 0,\ \ \forall z \in \mathcal{H}^1(\Sigma),\ \text{a.e. on } (0,\, T), \\ p(T) = k(y(T) - y_{_T}). \end{cases} \tag{3.5}$$

Combining (3.1) with (3.4), (3.5) we obtain

$$\delta J_k(v) = \int_{\omega\times(0,\,T)} (v + p)\, \delta v\, d\Sigma\, dt. \tag{3.6}$$

Since we also have ($\mathscr{U}$ being a Hilbert space for the inner-product $\{v, w\} \longrightarrow \int_{\omega\times(0,\,T)} v\, w\, d\Sigma\, dt$) $\delta J_k(v) = \int_{\omega\times(0,\,T)} DJ_k(v)\, \delta v\, d\Sigma\, dt$, it follows from (3.6) that

$$\boxed{DJ_k(v) = v + p|_{\omega\times(0,\,T)}.} \tag{3.7}$$

3.2 Optimality Conditions

Let u_k be the unique solution of the control problem (2.3), and denote by y_k and p_k the associated solution of (2.1) and (3.5), respectively. It follows from Section 3.1 that u_k is characterized by the following relations (the optimality system):

$$u_k + p_k|_{\omega\times(0,\,T)} = 0, \tag{3.8}$$

with

$$\begin{cases} \displaystyle\int_\Sigma \frac{\partial y_k}{\partial t}(t)\, z\, d\Sigma + \mu \int_\Sigma \nabla_\Sigma y_k(t) \cdot \nabla_\Sigma z\, d\Sigma = \int_\omega u_k(t) z\, d\Sigma,\ \forall z \in \mathcal{H}^1(\Sigma),\ \text{a.e. on } (0,\,T), \\ y_k(0) = y_0, \end{cases} \tag{3.9}$$

and

$$\begin{cases} \displaystyle -\int_\Sigma \frac{\partial p_k}{\partial t}(t)\, z\, d\Sigma + \mu \int_\Sigma \nabla_\Sigma p_k(t) \cdot \nabla_\Sigma z\, d\Sigma = 0,\ \forall z \in \mathcal{H}^1(\Sigma),\ \text{a.e. on } (0,\,T), \\ p_k(T) = k(y_k(T) - y_T). \end{cases} \tag{3.10}$$

Relations (3.8)–(3.10) clearly suggest the following approach (of the fixed *point type*) to solve the control problem (2.3):

(i) Let u_0 be a guess of u_k.

(ii) Denote by y_0 the solution of (2.1) associated with u_0.

(iii) Denote by p_0 the solution of (3.5) associated with y_0.

(iv) If $u_0 + p_0|_{\omega\times(0,\,T)}$ is small enough in $\mathscr{U}$ take $u_k = -p_0|_{\omega\times(0,\,T)}$; otherwise use appropriately the residual $u_0 + p_0|_{\omega\times(0,\,T)}$ to correct u_0, and repeat the process.

In Section 4 we will show that the above program can be achieved using a *conjugate gradient algorithm* operating in the space $\mathscr{U}$.

Remark 3.1. An alternative to the above approach (a *dual* of it in some sense, as shown in the Chapter 1 of [7]) can be defined as follows:

(i) Let e_0 be a guess of $y_k(T)$.

(ii) Denote by p_0 the solution of (3.5) verifying $p_0(T) = e_0$.

(iii) Denote by y_0 the solution of (2.1) associated with $u_0 = -p_0|_{\omega\times(0,\,T)}$.

(iv) If $e_0 - k(y_0(T) - y_T)$ is small enough in $\mathcal{L}^2(\Sigma)$ take $u_k = u_0$; otherwise use appropriately the residual $e_0 - k(y_0(T) - y_T)$ to correct e_0, and repeat the process.

This alternative approach can be implemented via a conjugate gradient algorithm operating in $\mathcal{L}^2(\Sigma)$. Variants of it have been tested in [7] and [2], to solve numerically approximate controllability problems for the heat equation in bounded domains of $\mathbb{R}^2$. In this article, we will solve directly problem (2.3) (the *primal problem*) using a conjugate gradient algorithm operating in the control space $\mathscr{U}$. The main reasons for preferring the direct approach to the dual one are that (a) it is conceptually simpler, and (b) it can be easily extended to nonlinear diffusion models, unlike the dual approach.

4 Conjugate Gradient Solution of Problem (2.3)

Problem (2.3) is a well–posed minimization problem in the control space $\mathscr{U}$ $(= \mathcal{L}^2(\omega \times (0, T))$, a real Hilbert space for the inner–product $\{v, w\} \to \int_{\omega\times(0,T)} v\, w\, d\Sigma\, dt$. It is therefore a particular case of those minimization problems in Hilbert space whose conjugate gradient solution is discussed in, e.g., the Chapter 1 of [7] and the Chapter 3 of [6] (see also the many references therein). Taking into account the results of Section 3, relation (3.7) in particular, the solution of problem (2.3) can be achieved by the following conjugate gradient algorithm (for notation convenience we denote by Y_0 the initial value we denoted by y_0 in the previous sections):

Step 1. Initialization: given

$$u_0 \text{ in } \mathscr{U}, \tag{4.1}$$

solve the following two problems.

$$\begin{cases} \displaystyle\int_\Sigma \frac{\partial y_0}{\partial t}(t)\, z\, d\Sigma + \mu \int_\Sigma \nabla_\Sigma y_0(t) \cdot \nabla_\Sigma z\, d\Sigma = \int_\omega u_0(t)\, z\, d\Sigma, \ \ \forall z \in \mathcal{H}^1(\Sigma), \text{ a.e. on } (0, T), \\ y_0(0) = Y_0, \end{cases} \tag{4.2}$$

$$\begin{cases} \displaystyle -\int_\Sigma \frac{\partial p_0}{\partial t}(t)\, z\, d\Sigma + \mu \int_\Sigma \nabla_\Sigma p_0(t) \cdot \nabla_\Sigma z\, d\Sigma = 0, \ \ \forall z \in \mathcal{H}^1(\Sigma), \text{ a.e. on } (0, T), \\ p_0(T) = k(y_0(T) - y_T). \end{cases} \tag{4.3}$$

Set $g_0 = u_0 + p_0|_{\omega\times(0,T)}$. If $\int_{\omega\times(0,T)} |g_0|^2 d\Sigma dt / \max\left[1, \int_{\omega\times(0,T)} |u_0|^2 d\Sigma dt\right] \le tol$, take $u_k = u_0$; otherwise set

$$d_0 = g_0. \tag{4.4}$$

Step 2. Descent: Then for $q \ge 0$, assuming that u_q, g_q, and d_q are known, the last two different from 0, we compute u_{q+1}, g_{q+1}, and if necessary, d_{q+1} as follows:
Solve

$$\begin{cases} \displaystyle\int_\Sigma \frac{\partial \overline{y}_q}{\partial t}(t)\, z\, d\Sigma + \mu \int_\Sigma \nabla_\Sigma \overline{y}_q(t) \cdot \nabla_\Sigma z\, d\Sigma = \int_\omega d_q(t) z\, d\Sigma, \ \ \forall z \in \mathcal{H}^1(\Sigma), \text{ a.e. on } (0, T), \\ \overline{y}_q(0) = 0, \end{cases} \tag{4.5}$$

$$\begin{cases} -\displaystyle\int_\Sigma \frac{\partial \overline{p}_q}{\partial t}(t)\, z\, d\Sigma + \mu \int_\Sigma \nabla_\Sigma \overline{p}_q(t) \cdot \nabla_\Sigma z\, d\Sigma = 0, \ \ \forall z \in \mathcal{H}^1(\Sigma), \text{ a.e. on } (0,\, T), \\ \overline{p}_q(T) = k\overline{g}_q(T), \end{cases} \tag{4.6}$$

and set

$$\overline{g}_q = d_q + \overline{p}_q|_{\omega\times(0,\,T)}. \tag{4.7}$$

Compute

$$\alpha_q = \frac{\displaystyle\int_{\omega\times(0,\,T)} |g_q|^2\, d\Sigma\, dt}{\displaystyle\int_{\omega\times(0,\,T)} d_q\, \overline{g}_q\, d\Sigma\, dt}, \tag{4.8}$$

and then

$$u_{q+1} = u_q - \alpha_q d_q, \tag{4.9}$$

$$g_{q+1} = g_q - \alpha_q \overline{g}_q. \tag{4.10}$$

Step 3. Testing the convergence. Construction of the new descent direction If $\int_{\omega\times(0,\,T)} |\, g_{q+1}|^2\, d\Sigma\, dt / \max\left[\int_{\omega\times(0,\,T)} |g_0|^2\, d\Sigma\, dt,\, \int_{\omega\times(0,\,T)} |u_{q+1}|^2\, d\Sigma\, dt\right] \leq tol$ take $u_k = u_{q+1}$; otherwise, compute

$$\beta_q = \frac{\displaystyle\int_{\omega\times(0,\,T)} |g_{q+1}|^2\, d\Sigma\, dt}{\displaystyle\int_{\omega\times(0,\,T)} |g_q|^2\, d\Sigma\, dt}, \tag{4.11}$$

and

$$d_{q+1} = g_{q+1} + \beta_q\, d_q. \tag{4.12}$$

Do $q+1 \longrightarrow q$ and return to Steep 2.

Concerning the choice of *tol*, following the Chapter 3 of [6], we advocate to take $tol = 10^d$ where d is the number of digits used for the floating point representation of the real numbers in the computer platform we use for our computations.

By a slight variant of the analysis done in the Chapter 1 of [7] for the "ordinary heat equation", one can prove that, for a given value of *tol*, the number of iterations, necessary to achieve the convergence of the above algorithm, varies like $\sqrt{k}$.

5 Discretization of the Control Problem (2.3) and Iterative Solution of the Fully Discrete Problem

5.1 Time discretization of the control problem (2.3)

With N a positive integer, we define the *time discretization step* Δt as $\Delta t = T/N$. Next, we approximate the control problem (2.3) by

$$\begin{cases} \mathbf{u}_k^{\Delta t} \in \mathscr{U}^{\Delta t}, \\ J_k^{\Delta t}(\mathbf{u}_k^{\Delta t}) \leq J_k^{\Delta t}(\mathbf{v}),\ \forall \mathbf{v} \in \mathscr{U}^{\Delta t}, \end{cases} \tag{5.1}$$

where $\mathscr{U}^{\Delta t} = \big(\mathcal{L}^2(\omega)\big)^N$, $\mathbf{u}_k^{\Delta t} = \{u_k^n\}_{n=1}^N$, $\mathbf{v} = \{v^n\}_{n=1}^N$, and the cost functional $J_k^{\Delta t}$ is defined by

$$J_k^{\Delta t}(\mathbf{v}) = \frac{\Delta t}{2} \sum_{n=1}^{N} \int_\omega |v^n|^2 \, d\Sigma \, + \, \frac{k}{2} \int_\Omega |y^N - y_T|^2 \, d\Sigma, \tag{5.2}$$

with $\{y^n\}_{n=1}^N$ defined from $\mathbf{v}$ and y_0 from the solution of:

$$y^0 = y_0, \tag{5.3}$$

for $n = 1, \ldots, N$

$$\begin{cases} y^n \in \mathcal{H}^1(\Sigma), \\ \displaystyle\int_\Sigma \frac{y^n - y^{n-1}}{\Delta t} z \, d\Sigma \, + \, \mu \int_\Sigma \nabla_\Sigma y^n \cdot \nabla_\Sigma z \, d\Sigma \, = \, \int_\omega v^n z \, d\Sigma, \;\; \forall z \in \mathcal{H}^1(\Sigma), \end{cases} \tag{5.4}$$

where $y^n = y(x, n\Delta t)$. Problems (5.4) are well-posed elliptic problems; strictly speaking they are not associated with any boundary condition since Σ is a surface *without* boundary.

Using classical *convexity* arguments, one can easily show that the discrete problem (5.1) has a unique solution, characterized by

$$DJ_k^{\Delta t}(\mathbf{u}_k^{\Delta t}) = \mathbf{0}, \tag{5.5}$$

where $DJ_k^{\Delta t}$ denotes the differential of $J_k^{\Delta t}$. Taking $\{\mathbf{v}, \mathbf{w}\} \to \Delta t \sum_{n=1}^N v^n w^v \; (= (\mathbf{v}, \mathbf{w})_{\Delta t})$ as inner–product over $\mathscr{U}^{\Delta t}$, and using a time–discrete variant of the perturbation method used in Section 3.1, we can show that

$$\big(DJ_k^{\Delta t}(\mathbf{v}), \mathbf{w}\big)_{\Delta t} = \Delta t \sum_{n=1}^{N} \int_\omega (v^n + p^n) \, w^n \, d\Sigma, \tag{5.6}$$

where $\{p^n\}_{n=1}^N$ is obtained from $\mathbf{v}$ via the solution of (5.3), (5.4) and of the following backward in time discrete initial value problem (the associated adjoint system):

$$p^{N+1} = k(y^N - y_T), \tag{5.7}$$

for $n = N, \ldots, 1$

$$\begin{cases} p^n \in \mathcal{H}^1(\Sigma), \\ \displaystyle\int_\Sigma \frac{p^n - p^{n+1}}{\Delta t} z \, d\Sigma \, + \, \mu \int_\Sigma \nabla_\Sigma p^n \cdot \nabla_\Sigma z \, d\Sigma \, = \, 0, \;\; \forall z \in \mathcal{H}^1(\Sigma), \end{cases} \tag{5.8}$$

where $p^n = p(x, n\Delta t)$. There is no basic difficulty at deriving a time–discrete analogue of the conjugate gradient algorithm (4.1)–(4.12), in order to solve the discrete control problem (5.1), via the optimality condition (5.5). In order to avoid being repetitious we will not describe this algorithm in this article, on the other hand we will describe a *fully-discrete* analogue of the two above algorithms in Section 5.2 after discussing, the space discretization of problem (5.2).

Remark 5.1. To time–discretize the parabolic problems (2.1) and (3.5), we have used the backward Euler scheme, obtaining thus (5.3), (5.4) and (5.7), (5.8). This implicit scheme is only first order accurate, but is stiff A–stable, robust and preserves the maximum principle if combined with appropriate space approximations. In [2] a second order accurate two step

backward implicit scheme has been used to solve related controllability problems for the classical heat equation; this scheme could have been used here also. The main reasons we did not are that: (a) the scheme does not preserve the maximum principle, (b) it requires a starting procedure, (c) deriving the associated discrete adjoint system is significantly more complicated than when using the backward Euler's scheme, d) if $\upsilon = 0$, as for the continuous model, the damping of the spectral modes of the solution increases monotonically with the value of the associated eigenvalues of the opposite of the Laplace–Beltrami operator, and e) (last but not least) a collaboration with NASA engineers working on the real time control of sub–systems of the Space Shuttle and International Space Station have shown us that most often the time–discretization method of choice for these engineers is the forward Euler's scheme with a fixed time–discretization step, chosen small enough to avoid numerical instabilities.

5.2 Full discretization of the control problem (2.3)

The time–discretization of problem (2.3) has been addressed in Section 5.1. Concerning the space–discretization we have two options:

(i) Approximate Σ by a *polyhedral surface* and proceed as in [1] to approximate the various elliptic problems encountered in (5.4), (5.8).

(ii) As in [8], use the parameterization associated with Figure 1, namely

$$\begin{cases} x_1 = (R + r\cos\theta)\cos\phi, \\ x_2 = (R + r\cos\theta)\sin\phi, \\ x_3 = r\sin\theta, \end{cases} \tag{5.9}$$

to map Σ over the square $\widehat{\Omega} = (0,\, 2\pi) \times (0,\, 2\pi)$ of the plane $(\phi,\, \theta)$, *periodic boundary conditions* being used to take into account the fact that Σ is without boundary. The problem being formulated on a planar domain, one can easily space–approximate it, using those finite element methods discussed in, e.g., the Appendix 1 of [5].

Using transformation (5.9), we clearly have

$$d\Sigma = r\,(R + r\cos\theta)\,d\phi d\theta, \tag{5.10}$$

$$\nabla_{\Sigma} y = \left[\frac{1}{R + r\cos\theta}\frac{\partial y}{\partial \phi},\, \frac{1}{r}\frac{\partial y}{\partial \theta}\right]. \tag{5.11}$$

Let denote by $\widehat{\omega}$ the pre–image of ω by the geometrical transformation defined by (5.9); the time–discrete control problem can be then reformulated as (keeping some of the notation unchanged):

$$\begin{cases} \mathbf{u}_k^{\Delta t} \in \mathscr{U}^{\Delta t}, \\ J_k^{\Delta t}(\mathbf{u}_k^{\Delta t}) \leq J_k^{\Delta t}(\mathbf{v}),\ \forall \mathbf{v} \in \mathscr{U}^{\Delta t}, \end{cases} \tag{5.12}$$

with $\mathscr{U}^{\Delta t} = \left(\mathcal{L}^2(\widehat{\omega})\right)^N$, the space $\mathscr{U}^{\Delta t}$ being equipped with the following inner–product $\{\mathbf{v}, \mathbf{w}\} \longrightarrow r\Delta t \sum_{n=1}^{N} \int_{\widehat{\omega}} v^n w^n (R + r\cos\theta)\, d\phi\, d\theta$ $(= (\mathbf{v},\, \mathbf{w})_{\Delta t})$. The cost functional $J_k^{\Delta t}$ is defined by

$$J_k^{\Delta t}(\mathbf{v}) = \frac{r}{2}\Delta t \sum_{n=1}^{N} \int_{\widehat{\omega}} |v^n|^2 (R + r\cos\theta)\, d\phi\, d\theta + \frac{k}{2} r \int_{\widehat{\Omega}} |y^N - y_{_T}|^2 (R + r\cos\theta)\, d\phi\, d\theta, \tag{5.13}$$

with $\{y^n\}_{n=1}^N$ obtained from y_0 and $\mathbf{v}$ via

$$y^0 = y_0, \tag{5.14}$$

for $n = 1, \ldots, N$ solve

$$\begin{cases} y^n \in \mathcal{H}_p^1(\widehat{\Omega}), \\ r\displaystyle\int_{\widehat{\Omega}} \frac{y^n - y^{n-1}}{\Delta t} z(R + r\cos\theta)\, d\phi\, d\theta \\ +\mu \displaystyle\int_{\widehat{\Omega}} \left(\frac{r}{R + r\cos\theta} \frac{\partial y^n}{\partial \phi} \frac{\partial z}{\partial \phi} + \frac{R + r\cos\theta}{r} \frac{\partial y^n}{\partial \theta} \frac{\partial z}{\partial \theta} \right) d\phi\, d\theta \\ = r\displaystyle\int_{\widehat{\omega}} v^n z(R + r\cos\theta)\, d\phi\, d\theta, \ \ \forall z \in \mathcal{H}_p^1(\widehat{\Omega}), \end{cases} \tag{5.15}$$

where

$$\mathcal{H}_p^1(\widehat{\Omega}) = \Big\{ z | z \in \mathcal{H}^1(\widehat{\Omega}),\ z(\phi,\, 0) = z(\phi,\, 2\pi) \text{ a.e. on } (0,\, 2\pi),\ z(0,\, \theta) = z(2\pi,\, \theta) \text{ a.e. on } (0,\, 2\pi) \Big\}.$$

The space $\mathcal{H}_p^1(\widehat{\Omega})$ is a space of doubly periodic functions, while (5.15) is a well–posed elliptic problem associated with an elliptic operator with smooth–varying *non–constant coefficients*.

The differential $DJ_k^{\Delta t}(\mathbf{v})$ of $J_k^{\Delta t}$ at $\mathbf{v} \in \mathscr{U}^{\Delta t}$ is given by

$$\big(DJ_k^{\Delta t}(\mathbf{v}),\, \mathbf{w}\big)_{\Delta t} = r\Delta t \sum_{n=1}^{N} \int_{\widehat{\omega}} (v^n + p^n)\, w^n (R + r\cos\theta)\, d\phi\, d\theta, \ \ \forall \mathbf{w} \in \mathscr{U}^{\Delta t}, \tag{5.16}$$

with $\{p^n\}_{n=1}^N$ obtained from y^N (and therefore from $\mathbf{v}$) via the solution of the following time–discrete adjoint system:

$$p^{N+1} = k(y^N - y_T), \tag{5.17}$$

for $n = N, \ldots, 1$, solve

$$\begin{cases} p^n \in \mathcal{H}_p^1(\widehat{\Omega}), \\ r\displaystyle\int_{\widehat{\Omega}} \frac{p^n - p^{n+1}}{\Delta t} z(R + r\cos\theta)\, d\phi\, d\theta \\ +\mu \displaystyle\int_{\widehat{\Omega}} \left(\frac{r}{R + r\cos\theta} \frac{\partial p^n}{\partial \phi} \frac{\partial z}{\partial \phi} + \frac{R + r\cos\theta}{r} \frac{\partial p^n}{\partial \theta} \frac{\partial z}{\partial \theta} \right) d\phi\, d\theta \ = \ 0, \\ \forall z \in \mathcal{H}_p^1(\widehat{\Omega}). \end{cases} \tag{5.18}$$

The solution of problem (5.12) is characterized by $DJ_k^{\Delta t}(\mathbf{u}_k^{\Delta t}) = \mathbf{0}$.

These preliminaries being done we can address now the full discretization of the control problem (2.3). The first step in that direction is the approximation of $\mathcal{H}_p^1(\widehat{\Omega})$. In this article we advocate using *finite element approximations*, since they are well–suited to the fact that the state and co–state equations have been given directly in variational forms. We consider thus a finite element triangulation $\mathcal{T}_h$ of $\widehat{\Omega}$ with the following classical properties (see, e.g., the Appendix 1 of [5] and the references therein):

(i) $\mathcal{T}_h$ is a finite collection of closed triangles K contained in $\overline{\widehat{\Omega}}$, with h denoting the length of the largest edge(s) of $\mathcal{T}$, and where (ii) $\overline{\widehat{\Omega}} = \bigcup_{K \in \mathcal{T}_h} K$. (iii) If K and K' belong to $\mathcal{T}_h$, with $K \neq K'$, we have either $K \cap K' = \emptyset$, or K and K' have only one vertex in common, or one full edge in common. Here, since we are dealing with spaces of doubly periodic functions, $\mathcal{T}_h$ has to satisfy the additional property: (iv) The vertices of $\mathcal{T}_h$ located

on the edge $\{\{\phi,\,\theta\}\,|\,\phi=2\pi,\,\theta\in[0,\,2\pi]\}$ of $\overline{\widehat{\Omega}}$ are obtained from those located on the edge $\{\{\phi,\,\theta\}\,|\,\phi=0,\,\theta\in[0,\,2\pi]\}$ by a 2π–translation parallel to the axis $O\phi$. A similar property holds for the two other edges of $\overline{\widehat{\Omega}}$. A triangulation verifying the above assumption has been visualized in Figure 2 below:

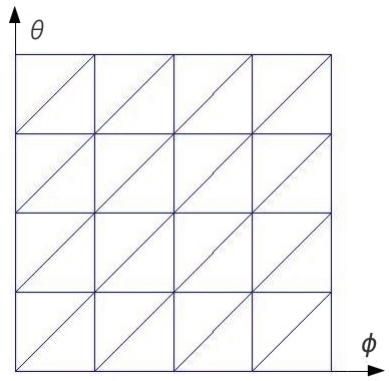

Figure 2: A triangulation of $\overline{\widehat{\Omega}}$

We approximate then $\mathcal{H}_p^1(\widehat{\Omega})$ by

$$V_h=\Big\{z\,|\,z\in\mathcal{C}^0(\overline{\widehat{\Omega}}),\,z|_K\in\mathbb{P}_1,\,\forall K\in\mathcal{T}_h,z(0,\,\theta)=z(2\pi,\,\theta),\,z(\phi,\,0)=z(\phi,\,2\pi),\\ \forall\{\phi,\,\theta\}\in[0,\,2\pi]^2\Big\}\quad(5.19)$$

where, in (5.19), $\mathbb{P}_1$ is the space of the two variable polynomials of degree ≤ 1.

Hereafter, we will assume that $\overline{\widehat{\omega}}$ is also the union of triangles of $\mathcal{T}_h$, a reasonable simplification which allows us to fully approximate the control problem (2.3) by

$$\begin{cases}\mathbf{u}_{kh}^{\Delta t}\in\mathscr{U}_h^{\Delta t},\\ J_{kh}^{\Delta t}(\mathbf{u}_{kh}^{\Delta t})\leq J_{kh}^{\Delta t}(\mathbf{v}),\,\forall\mathbf{v}\in\mathscr{U}_h^{\Delta t},\end{cases}\quad(5.20)$$

where in (5.20) the fully discrete control space $\mathscr{U}_h^{\Delta t}$ is defined by

$$\mathscr{U}_h^{\Delta t}=\Big\{\mathbf{v}\,|\,\mathbf{v}=\{v_h^n\}_{n=1}^N,\,v_h^n\in V_h|_{\overline{\widehat{\omega}}}\Big\},\quad(5.21)$$

and it is equipped with the inner–product

$$\{\mathbf{v},\mathbf{w}\}\to r\Delta t\sum_{n=1}^N\int_{\widehat{\omega}}v_h^n\,w_h^n(R+r\cos\theta)\,d\phi\,d\theta,\quad(5.22)$$

that we will denote by $(\cdot,\,\cdot)_h^{\Delta t}$. We denote by $\mathcal{T}_{\widehat{\omega}h}$ the subset of $\mathcal{T}_h$ defined by

$$\mathcal{T}_{\widehat{\omega}h}=\Big\{K\,|\,K\in\mathcal{T}_h,\,K\subset\overline{\widehat{\omega}}\Big\}.$$

The cost functional $J_{kh}^{\Delta t}$ is defined by

$$J_{kh}^{\Delta t}(\mathbf{v}) = \frac{r}{2}\Delta t \sum_{n=1}^{N} \int_{\widehat{\omega}} |v_h^n|^2 (R + r\cos\theta)\, d\phi\, d\theta \,+\, \frac{k}{2} r \int_{\widehat{\Omega}} |y_h^N - y_T|^2 (R + r\cos\theta)\, d\phi\, d\theta, \quad (5.23)$$

with $\{y_h^n\}_{n=1}^N$ obtained from y_0 and $\mathbf{v}$ via solution of

$$y_h^0 = y_{0h}\, (\in V_h). \quad (5.24)$$

For $n = 1, \ldots, N$ solve

$$\begin{cases} y_h^n \in V_h \\ r \displaystyle\int_{\widehat{\Omega}} \frac{y_h^n - y_h^{n-1}}{\Delta t} z (R + r\cos\theta)\, d\phi\, d\theta \\ + \mu \displaystyle\int_{\widehat{\Omega}} \left(\frac{r}{R + r\cos\theta} \frac{\partial y_h^n}{\partial \phi} \frac{\partial z}{\partial \phi} \,+\, \frac{R + r\cos\theta}{r} \frac{\partial y_h^n}{\partial \theta} \frac{\partial z}{\partial \theta} \right) d\phi\, d\theta \\ = \; r \displaystyle\int_{\widehat{\omega}} v_h^n z (R + r\cos\theta)\, d\phi\, d\theta, \;\; \forall z \in V_h, \end{cases} \quad (5.25)$$

where y_{0h} is an approximation of y_0 belonging to V_h.

Remark 5.2. For the computations whose results will be presented in Section 6, we have employed the *trapezoidal rule* on each triangle of $\mathcal{T}_h$ and $\mathcal{T}_{\widehat{\omega}h}$ to approximate the integrals encountered in (5.22), (5.23) and (5.25), taking advantage of

$$\int_{\widehat{\Omega}} = \sum_{K \in \mathcal{T}_h} \int_K, \quad \text{and} \quad \int_{\widehat{\omega}} = \sum_{K \in \mathcal{T}_{\widehat{\omega}h}} \int_K. \quad \square$$

Proceeding as in Section 3, we can show that the differential $DJ_{kh}^{\Delta t}(\mathbf{v})$ of $J_{kh}^{\Delta t}$ at $\mathbf{v}$ is defined by

$$\left(DJ_h^{\Delta t}(\mathbf{v}),\, \mathbf{w}\right)_h^{\Delta t} = r\Delta t \sum_{n=1}^{N} \int_{\widehat{\omega}} (v_h^n + p_h^n)\, w_h^n (R + r\cos\theta)\, d\phi\, d\theta, \;\; \forall\, \mathbf{w} \in \mathscr{U}_h^{\Delta t}, \quad (5.26)$$

with $\{p_h^n\}_{n=1}^N$ obtained from the solution of the fully discrete adjoint problem

$$p_h^{N+1} = k(y_h^N - y_{Th}). \quad (5.27)$$

For $n = N, \ldots, 1$, solve

$$\begin{cases} p_h^n \in V_h, \\ r \displaystyle\int_{\widehat{\Omega}} \frac{p_h^n - p_h^{n+1}}{\Delta t} z (R + r\cos\theta)\, d\phi\, d\theta \\ + \mu \displaystyle\int_{\widehat{\Omega}} \left(\frac{r}{R + r\cos\theta} \frac{\partial p_h^n}{\partial \phi} \frac{\partial z}{\partial \phi} + \frac{R + r\cos\theta}{r} \frac{\partial p_h^n}{\partial \theta} \frac{\partial z}{\partial \theta} \right) d\phi\, d\theta \;=\; 0, \\ \forall z \in V_h \end{cases} \quad (5.28)$$

in (5.27), y_{Th} is an approximation of y_T belonging to V_h. It follows from (5.26) that

$$DJ_h^{\Delta t}(\mathbf{v}) = \{v_h^n + p_h^n|_{\widehat{\omega}}\}_{n=1}^N. \quad (5.29)$$

The solution $\mathbf{u}_{kh}^{\Delta t}$ of problem (5.23) is characterized by

$$DJ_{kh}^{\Delta t}(\mathbf{u}_{kh}^{\Delta t}) = \mathbf{0}. \tag{5.30}$$

Remark 5.2 applies also to the integrals in (5.26) and (5.28).

Taking advantage of (5.26) and (5.29), it makes sense to solve the fully discrete control problem (5.20) via the solution of (5.30). This solution can be achieved by a *conjugate gradient algorithm*, which is nothing but the *fully discrete* version of algorithm (4.1)–(4.12) discussed in Section 4. This new conjugate gradient algorithm reads as follows:

$$\text{Given } \mathbf{u}_0 = \{u_0^n\}_{n=1}^N \text{ in } \mathscr{U}_h^{\Delta t}, \tag{5.31}$$

solve

$$\begin{cases} y_0^0 = y_{0h}; \\ \text{for } n = 1, \ldots, N, \text{ solve} \\ \begin{cases} y_0^n \in V_h, \\ r\displaystyle\int_{\widehat{\Omega}} \frac{y_0^n - y_0^{n-1}}{\Delta t} z(R + r\cos\theta)\, d\phi\, d\theta \\ + \mu \displaystyle\int_{\widehat{\Omega}} \left(\frac{r}{R + r\cos\theta} \frac{\partial y_0^n}{\partial \phi} \frac{\partial z}{\partial \phi} + \frac{R + r\cos\theta}{r} \frac{\partial y_0^n}{\partial \theta} \frac{\partial z}{\partial \theta} \right) d\phi\, d\theta \; = \\ r\displaystyle\int_{\widehat{\omega}} u_0^n z(R + r\cos\theta)\, d\phi\, d\theta, \;\; \forall z \in V_h, \end{cases} \end{cases} \tag{5.32}$$

and

$$\begin{cases} p_0^{N+1} = k(y_0^N - y_{Th}); \\ \text{for } n = N, \ldots, 1, \text{ solve} \\ \begin{cases} p_0^n \in V_h, \\ r\displaystyle\int_{\widehat{\Omega}} \frac{p_0^n - p_0^{n+1}}{\Delta t} z(R + r\cos\theta)\, d\phi\, d\theta \\ + \mu \displaystyle\int_{\widehat{\Omega}} \left(\frac{r}{R + r\cos\theta} \frac{\partial p_0^n}{\partial \phi} \frac{\partial z}{\partial \phi} + \frac{R + r\cos\theta}{r} \frac{\partial p_0^n}{\partial \theta} \frac{\partial z}{\partial \theta} \right) d\phi\, d\theta = \; 0, \\ \forall z \in V_h, \end{cases} \end{cases} \tag{5.33}$$

Define $\mathbf{g}_0 = \{g_0^n\}_{n=1}^N$ by

$$g_0^n = u_0^n + p_0^n|_{\widehat{\omega}}, \; \forall n = 1, \ldots, N. \tag{5.34}$$

If $\frac{r\Delta t \sum_{n=1}^N \int_{\widehat{\omega}} |g_0^n|^2 (R + r\cos\theta)\, d\phi\, d\theta}{\max\left[1, r\Delta t \sum_{n=1}^N \int_{\widehat{\omega}} |u_0^n|^2 (R + r\cos\theta)\, d\phi\, d\theta\right]} \leq tol$, take $\mathbf{u}_{kh}^{\Delta t} = \mathbf{u}_0$; otherwise set

$$\mathbf{d}_0 = \mathbf{g}_0. \tag{5.35}$$

For $q \geq 0$, assuming that $\mathbf{u}_q$, $\mathbf{g}_q$, and $\mathbf{d}_q$ are known, the last two different from $\mathbf{0}$, we compute $\mathbf{u}_{q+1}$, $\mathbf{g}_{q+1}$, and, if necessary, $\mathbf{d}_{q+1}$ as follows:

Solve

$$\begin{cases} \overline{y}_q^0 = 0; \\ \text{for } n = 1, \dots, N, \text{ solve} \\ \begin{cases} \overline{y}_q^n \in V_h, \\ r \displaystyle\int_{\widehat{\Omega}} \frac{\overline{y}_q^n - \overline{y}_q^{n-1}}{\Delta t} z(R + r\cos\theta)\, d\phi\, d\theta \\ + \mu \displaystyle\int_{\widehat{\Omega}} \left(\frac{r}{R + r\cos\theta} \frac{\partial \overline{y}_q^n}{\partial \phi} \frac{\partial z}{\partial \phi} + \frac{R + r\cos\theta}{r} \frac{\partial \overline{y}_q^n}{\partial \theta} \frac{\partial z}{\partial \theta} \right) d\phi\, d\theta \\ = r \displaystyle\int_{\widehat{\omega}} d_q^n z(R + r\cos\theta)\, d\phi\, d\theta, \ \ \forall z \in V_h, \end{cases} \end{cases} \tag{5.36}$$

and

$$\begin{cases} \overline{p}_q^{N+1} = k\overline{y}_q^N; \\ \text{for } n = N, \dots, 1, \text{ solve} \\ \begin{cases} \overline{p}_q^n \in V_h, \\ r \displaystyle\int_{\widehat{\Omega}} \frac{\overline{p}_q^n - \overline{p}_q^{n+1}}{\Delta t} z(R + r\cos\theta)\, d\phi\, d\theta \\ + \mu \displaystyle\int_{\widehat{\Omega}} \left(\frac{r}{R + r\cos\theta} \frac{\partial \overline{p}_q^n}{\partial \phi} \frac{\partial z}{\partial \phi} + \frac{R + r\cos\theta}{r} \frac{\partial \overline{p}_q^n}{\partial \theta} \frac{\partial z}{\partial \theta} \right) d\phi\, d\theta = 0, \\ \forall z \in V_h. \end{cases} \end{cases} \tag{5.37}$$

Compute

$$\overline{\mathbf{g}}_q = \{\overline{g}_q^n\}_{n=1}^N = \{d_q^n + \overline{p}_q^n|_{\widehat{\omega}}\}_{n=1}^N, \tag{5.38}$$

$$\alpha_q = \sum_{n=1}^N \int_{\widehat{\omega}} |g_q^n|^2 (R + r\cos\theta)\, d\phi\, d\theta \Big/ \sum_{n=1}^N \int_{\widehat{\omega}} \overline{g}_q^n\, d_q^n (R + r\cos\theta)\, d\phi\, d\theta, \tag{5.39}$$

$$\mathbf{u}_{q+1} = \mathbf{u}_q - \alpha_q \mathbf{d}_q, \tag{5.40}$$

$$\mathbf{g}_{q+1} = \mathbf{g}_q - \alpha_q \overline{\mathbf{g}}_q. \tag{5.41}$$

If $\dfrac{\sum_{n=1}^N \int_{\widehat{\omega}} |g_{q+1}^n|^2 (R + r\cos\theta)\, d\phi\, d\theta}{\max\left[\sum_{n=1}^N \int_{\widehat{\omega}} |g_0^n|^2 (R + r\cos\theta)\, d\phi\, d\theta\, , \sum_{n=1}^N \int_{\widehat{\omega}} |u_{q+1}^n|^2 (R + r\cos\theta)\, d\phi\, d\theta\right]} \leq tol$, take $\mathbf{u}_{kh}^{\Delta t} = \mathbf{u}_{q+1}$; otherwise compute

$$\beta_q = \sum_{n=1}^N \int_{\widehat{\omega}} |g_{q+1}^n|^2 (R + r\cos\theta)\, d\phi\, d\theta \Big/ \sum_{n=1}^N \int_{\widehat{\omega}} |g_q^n|^2 (R + r\cos\theta)\, d\phi\, d\theta, \tag{5.42}$$

and

$$\mathbf{d}_{q+1} = \mathbf{g}_{q+1} + \beta_q \mathbf{d}_q. \tag{5.43}$$

Do $q + 1 \longrightarrow q$ and return to (5.36).

Remark 5.2 still applies for the various integrals encountered in algorithm (5.31)–(5.43). Futher remarks are in order, among them:

Remark 5.3. The various discrete linear elliptic problems occurring in (5.32), (5.33) and (5.36), (5.37) are all associated with the same matrix, differing only by their right–hand sides. Since the above matrix is symmetric, positive definite and sparse, the associated linear systems can be solved by a sparse Cholesky solver, like the one available in MATLAB®. An alternative to Cholesky is to use a conjugate gradient algorithm initialized by the solution

at the previous time step. The backward Euler time discretization scheme that we employ being only first order accurate, using a small Δt is recommended, implying that the matrix associated with the backward Euler scheme is not too badly conditioned, authorizing thus the solution of these discrete elliptic problems by a conjugate gradient algorithm preconditioned by the diagonal of the above matrix. In this article we have solved these linear systems using one of those user friendly MATLAB® routines which decide 'by themselves' of the solver which is the most appropriate for the linear system under consideration.

Remark 5.4. The conjugate gradient algorithm (5.31)–(5.43) is a solver for (5.30), a linear problem in $\mathscr{U}_h^{\Delta t}$. For large values of the penalization parameter k the condition number of the linear operator associated with $DJ_{kh}^{\Delta t}$ is of the order of k, implying that the linear problem (5.30) is poorly conditioned making its solution by algorithm (5.31)–(5.43) sensitive to round–off errors. This explains that if we take the stopping criterion *tol* in (5.31)–(5.43) too small, the convergence properties of the above conjugate gradient algorithm will deteriorate. To avoid this situation we have taken *tol* significantly larger than the value advocated in Section 4 (we took *tol* of the order of 10^{-5} for our computations).

6 Numerical Examples

In this section we present some numerical results obtained using the methodology discussed above. We consider two types of controllability problems, namely: 1) Approximate controllability problems, where the control function is supported by a subdomain of the torus; 2) Null controllability problems, where the target function is $y_T = 0$.

6.1 Approximate distributed control problem

Experiments with a smooth target

We consider the surface of a torus with minor radius $r = 1$ and major radius $R = 2$. We first consider the smooth target,

$$y_T(\phi, \theta) = \cos\phi + \sin\theta, \tag{6.1}$$

with $\{\phi, \theta\} \in \widehat{\Omega} = (0, 2\pi)^2$. Here we chose $y_0 = 0$, $\mu = 2$ and $T = 2$ in equation (2.1). In the following numerical experiments the control is supported by strip–like subdomains $\widehat{\omega}$, which may have a vertical sweep $(\phi_f - \phi_0)$ with $\widehat{\omega} = (\phi_0, \phi_f) \times (0, 2\pi)$, or a horizontal sweep $(\theta_f - \theta_0)$ with $\widehat{\omega} = (0, 2\pi) \times (\theta_0, \theta_f)$. Figure 3 shows typical subdomains of each type on the surface Σ. To simplify, we will just call 'vertical subdomain' to vertical strip–like subdomains, and similarly for horizontal ones.

We first present numerical results where the control is supported by the horizontal subdomain $\widehat{\omega} = (0, 2\pi) \times (\pi/2, 3\pi/2)$, and where different values of Δt are employed in the conjugate gradient algorithm (5.31)–(5.43). Also, different regular uniform meshes on $\widehat{\Omega}$ are considered for the finite element discretization, with $\Delta\phi = \Delta\theta$ (see Fig. 2). The stopping criterion for the conjugate gradient algorithm is fixed at $tol = 5 \times 10^{-5}$. In these experiments we have taken $\mathbf{u}_0 = \mathbf{0}$ as initial guess, and $k = 10^8$ as value of the penalty parameter. The corresponding numerical results have been summarized in Table 1, where u^c and y^c denote the computed optimal control and the corresponding computed state, respectively, and, *No. iters* denotes the number of iterations necessary to achieve convergence of the conjugate gradient algorithm for the above tolerance, $Norm\, u^c$ is $||u^c||_{\mathcal{L}^2(\widehat{\omega}\times(0,T))}$ and *Rel. error* denotes the relative difference between the exact and computed target given

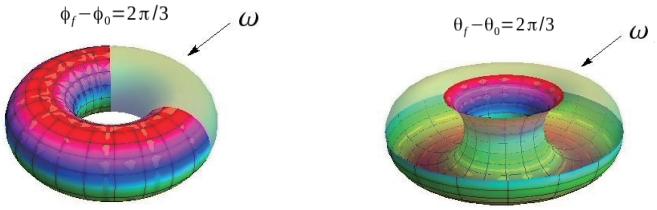

Figure 3: Domains of control: vertical sweep (left) and horizontal sweep (right).

Table 1: Summary of convergence results, with $\widehat{\omega} = (0,\, 2\pi) \times (\pi/2,\, 3\pi/2)$ and $\Delta\phi = \Delta\theta$

$\Delta\phi$	$2\pi/48$	$2\pi/72$	$2\pi/96$	$2\pi/108$	$2\pi/48$	$2\pi/96$
Δt	$1/100$	$1/100$	$1/100$	$1/100$	$1/200$	$1/200$
No. iters	29	28	27	26	29	27
Norm u^c	36.3334	37.0708	37.6837	37.8554	37.8081	37.6194
Rel. error	0.0161	0.0163	0.0161	0.0160	0.0172	0.0168

by $||y_T - y^c(T)||_{\mathcal{L}^2(\widehat{\Omega})}/||y_T||_{\mathcal{L}^2(\widehat{\Omega})}$. This table shows that the different values for the chosen discretization parameters lead to very close results, suggesting convergence with respect space–time discretization. In particular, the computed target function differs of the exact target by about 1.6% in most cases. Therefore, we decided to fix the discretization parameters at $\Delta t = 1/100$ and $\Delta\phi = \Delta\theta = 2\pi/48$, for the smooth target function under consideration.

Table 2 shows the influence of the penalty parameter on the numerical results, showing the convergence of $y_k(T)$ to y_T when $k \longrightarrow +\infty$. Different supporting subdomains ω are considered in this experiments. These results show that for increasing $|\omega|$ the numerical solutions is less sensitive to the value of k. Furthermore, we found that for $k > 10^8$ the numerical results are essentially the same for all cases. Thus, we will not consider values of k greater than 10^8 in the sequel.

Figure 4 shows the $\mathcal{L}^2$–norm of the computed control u^c versus time for different values of k for the case $\widehat{\omega} = (0, 2\pi) \times (2\pi/3, 4\pi/3)$. This figure exhibits the oscillation of the control function near T as for the heat case in [7] and [12].

Vertical supporting subdomains are not as good to obtain reasonable results as the horizontal ones. For instance, the results for all horizontal supporting subdomains in Table 2, except the last one, are better than the corresponding results for the vertical supporting subdomain $\widehat{\omega} = (0, \pi) \times (0, 2\pi)$, as it is easily realized looking at Table 3. This behavior may be associated with the fact that for $|\omega|$ small enough and R/r sufficiently large, the average distance (along the geodesics) of the points of Σ to the control supporting domain ω is smaller when ω is a horizontal strip, compared to when it is a vertical one (indeed, the length scale along the vertical directions is of the order πr, while it is πR in the horizontal directions).

Experiments with a non–smooth target

Now, for the next set of experiments we consider a non–smooth target, defined by the following function:

$$y_T = |\cos\phi| + |\sin\theta|. \tag{6.2}$$

Table 2: Numerical results for different horizontal strip–liked subdomains.

$\widehat{\omega}$	$\lvert\omega\rvert/\lvert\Omega\rvert$	k	*No. Iters*	*Norm* u^c	*Rel. error*
$(0,2\pi)\times(0,2\pi)$	1	10^4	5	14.5960	0.0033
		10^6	5	14.5469	0.0033
		10^8	5	14.5470	0.0033
$(0,2\pi)\times(\pi/2,3\pi/2)$	0.3408	10^4	19	34.3037	0.0269
		10^6	20	34.7010	0.0258
		10^8	20	34.7332	0.0258
$(0,2\pi)\times(2\pi/3,4\pi/3)$	0.1955	10^4	23	61.1809	0.0392
		10^6	26	64.8340	0.0312
		10^8	26	64.8657	0.0312
$(0,2\pi)\times(3\pi/4,5\pi/4)$	0.1375	10^4	25	84.0090	0.0582
		10^6	41	96.5666	0.0298
		10^8	41	96.6947	0.0297
$(0,2\pi)\times(7\pi/8,9\pi/8)$	0.0641	10^4	35	153.5422	0.1203
		10^6	41	205.1510	0.0539
		10^8	47	207.1548	0.0513
$(0,2\pi)\times(15\pi/16,17\pi/16)$	0.0320	10^4	39	204.3826	0.2504
		10^6	54	358.7140	0.0937
		10^8	54	363.1198	0.0925

Table 3: Numerical results for a vertical strip–liked subdomain.

$\widehat{\omega}$	$\lvert\omega\rvert/\lvert\Omega\rvert$	k	*No. Iters*	*Norm* u^c	*Rel. error*
$(0,\pi)\times(0,2\pi)$	0.5	10^4	72	92.5621	0.1223
		10^6	108	131.8721	0.0731
		10^8	108	132.3743	0.0729

Again, we choose the major radius $R = 2$ and the minor radius $r = 1$. The initial state is chosen as $y_0 = 0$ and we pick $T = 2$. Table 4 shows the numerical results for different values of μ when the control is supported by the strip–like horizontal subdomain $\widehat{\omega} = (0, 2\pi) \times (\pi/2, 3\pi/2)$, which satisfies $|\omega|/|\Omega| = 0.3408$, and different values of the discretization parameters Δt and $\Delta\phi = \Delta\theta$. The initial guess in the conjugate gradient iterations is $\mathbf{u}_0 = \mathbf{0}$, the value of the penalty parameter is $k = 10^8$ and the stopping criterion is fixed at $tol = 5 \times 10^{-5}$. This table shows that different values of the discretization parameters lead to very similar results for each value of μ, thus showing convergence with respect to numerical discretization. The results of Table 4 suggest that there exists an optimal value of μ (for ω and T given), minimizing the norm of the control. This is not surprising, since when μ is large, the 'natural' tendency of the system is to drive the solution quickly to $\bar{y}_0 = \frac{1}{|\Sigma|}\int_\Sigma y_0\, d\Sigma$, a phenomenon the control has to fight (unless $y_T = \bar{y}_0$), while small values of μ will imply that a long time is needed for the action of the control to affect significantly those points of Σ, away from ω. Indeed, we were not able to obtain, numerically, convergent results for $\mu = 1/8$ with $T = 2$ and the given supporting set $\widehat{\omega}$, even with a finer mesh in space and time. Actually, for smaller values of μ, a larger T or a larger supporting set for the control is required. Table 5 shows results with larger $\widehat{\omega}$. As expected, if $\omega = \Omega$ we can control the system with any value of μ and T. We want to emphasize that it is not necessary to use a finer mesh (in space and time) to get significant better results.

We now investigate the effect of T on the controllability, with different values of μ. We

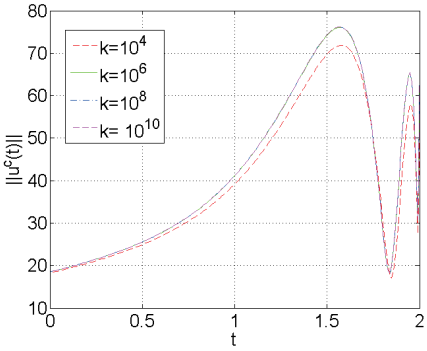

Figure 4: Norm of the computed control vs *time* for $k = 10^4$, 10^6, 10^8, 10^{10} for $\widehat{\omega} = (0, 2\pi) \times (2\pi/3, 4\pi/3)$.

Table 4: Summary of convergence results, with $\widehat{\omega} = (0,\, 2\pi) \times (\pi/2,\, 3\pi/2)$ and $\Delta\phi = \Delta\theta$

μ	$\Delta\phi$ / Δt	$2\pi/72$ / $1/100$	$2\pi/96$ / $1/100$	$2\pi/108$ / $1/100$	$2\pi/96$ / $1/200$	$2\pi/108$ / $1/200$
2	*No. iters*	22	17	18	20	19
	Norm u^c	39.7510	39.7861	39.6623	39.5984	39.6021
	Rel. error	0.0676	0.0685	0.0691	0.0695	0.0699
1	*No. iters*	18	15	15	18	16
	Norm u^c	29.9848	29.9491	30.0671	30.5332	30.3434
	Rel. error	0.0635	0.0651	0.0668	0.0668	0.0674
1/2	*No. iters*	21	17	17	21	20
	Norm u^c	31.74084	31.4472	31.2907	32.8792	32.6179
	Rel. error	0.0568	0.0586	0.0599	0.0577	0.0578
1/4	*No. iters*	28	25	25	34	30
	Norm u^c	53.5163	52.6179	52.7648	57.6699	55.9594
	Rel. error	0.0770	0.0784	0.0783	0.0806	0.0817

picked $\Delta t = 1/100$ and $\Delta\phi = \Delta\theta = 2\pi/108$. The values of r, R, k and *tol* are the same as in the previous examples. The numerical results are summarized in Table 6. All results were obtained with the supporting set $\widehat{\omega}_1 = (0,\, 2\pi) \times (\pi/2\, 3\pi/2)$. This table shows that there is a loss accuracy as T and μ get smaller. Apparently, a value of μT close to $1/4$ is critical for the given supporting set and the numerical methodology employed. In fact, in order to obtain a convergent solution for $\mu T < 1/4$ we need to consider a larger control supporting set. For instance, for $\mu = 1/2$ and $T = 1/4$ we obtained a convergent result with the larger supporting set $\widehat{\omega}_2 = (0,\, 2\pi) \times (\pi/2,\, 2\pi)$, as shown in Table 7.

Next, we study the controllability properties for three different horizontal–like supports with the same surface measure $|\omega|$. For these experiments we consider $\mu = 1/2$ and $T = 2$. The discretization parameters are the same as in the previous experiment, as well as the other parameters. Table 8 shows the results for two sets of experiments: the first three cases have surface area $|\omega| = 4\pi(\pi - 1)$, and the last three cases have surface area $|\omega| = 2\pi(\pi - 1)$. The behavior is not independent of the control zone, since the number of conjugate gradient iterations, to achieve convergence, is different for each case. However the relative errors are similar for each set of experiments.

In order to study the influence of R and r on the controllability, we consider the sup-

Table 5: Results for smaller values of μ

μ	$\widehat{\omega}$	$\lvert\omega\rvert/\lvert\Omega\rvert$	*No. iters.*	*Norm* u^c	*Rel.error*
1/8	$(0, 2\pi) \times (0, 3\pi/2)$	0.6704	39	31.5961	0.0364
1/25	$(0, 2\pi) \times (0, 5.5)$	0.8192	31	14.8281	0.0307
1/10000	$\widehat{\Omega}$	1	2	8.4977	0.0039

Table 6: Numerical results for different values of T and μ.

μ	T	$\lvert\omega\rvert/\lvert\Omega\rvert$	*No. Iters*	*Norm* u^c	*Rel.error*
1	2	0.3408	15	30.0671	0.0668
	1	0.3408	13	42.4999	0.0674
	1/2	0.3408	27	106.0272	0.0670
	1/4	0.3408	197	546.0387	0.0940
1/2	2	0.3408	17	31.2907	0.0599
	1	0.3408	27	74.9730	0.0670
	1/2	0.3408	190	377.8660	0.1067
1/4	2	0.3408	25	52.7048	0.0783
	1	0.3408	91	197.4128	0.1445
1/8	2	0.3408	86	140.1057	0.1445

porting subdomain $\widehat{\omega} = (0, 2\pi) \times (\pi/2, 3\pi/2)$, and parameters $\mu = 1/2$, $T = 2$. The discretization parameters are the same as before. First, we fixed R at 2 and let $r/R \longrightarrow 0^+$; results are summarized in Table 9. It can be observed that when r gets smaller the relative difference between $y_{_T}$ and $y^c(T)$ increases. This may be explained by the effect of diffusion: if μ is fixed, then diffusion plays a stronger role when the surface area gets smaller, and consequently it is more difficult to control the system. On the other hand, when the surface area of the torus increases, the opposite is true, as shown in Table 10. In this case, it is obvious that less iterations are needed to get the same accuracy, as R increases. Actually, with $\mu = 1/2$ and $T = 2$, the diffusion length scale $\approx \sqrt{\mu T} = 1$ is smaller than the size of the torus when $r = 1$ and $R > 1$. Thus, the size of the supporting set $|\omega|$ may be kept fixed as R increases without affecting the controllability of the system. To verify this behavior, we consider the following supporting sets on different torus of increasing size:

$$\begin{aligned}
\widehat{\omega}_1 &= (0,\, 2\pi) \times (\pi,\, 5.5991) \quad \text{for } R = 2,\\
\widehat{\omega}_2 &= (0,\, 2\pi) \times (\pi,\, 4.4551) \quad \text{for } R = 4,\\
\widehat{\omega}_3 &= (0,\, 2\pi) \times (\pi,\, 3.7483) \quad \text{for } R = 8.
\end{aligned}$$

All of them have the same surface area, $|\omega| = 4\pi(\pi - 1)$. Table 11 shows that there is no loss of accuracy, even though the ratio $|\omega|/|\Omega|$ decreases as R gets larger.

6.2 Null–controllability

The last set of numerical experiments presented in this article is concerned with test problems where the target function is $y_{_T} = 0$ (the null state). Let us recall that a system has the *null–controllability property* if it can be driven from any initial state y_0, to the null–state in finite time. Since the natural tendency of an uncontrolled diffusive system over Σ is to produce solutions converging to 0 as $t \longrightarrow +\infty$ (if we assume that $\int_\Sigma y_0 d\Sigma = 0$), it is reasonable to conjecture that these systems have the null controllability property. Indeed, it is proved in [9]

Table 7: Numerical result for $T = 1/4$ on $\widehat{\omega} = (0,\, 2\pi) \times (\pi/2,\, 2\pi)$.

μ	T	$\lvert\omega\rvert/\lvert\Omega\rvert$	*No. Iters*	*Norm* u^c	*Rel.error*
1/2	1/4	0.6704	48	179.7166	0.0771

Table 8: Numerical results for different supports with the same measure surface $|\omega|$.

Supporting set $\widehat{\omega}$	$\lvert\omega\rvert/\lvert\Omega\rvert$	*No. Iters*	*Norm* u^c	*Rel. error*	*Rel. error/Norm* u^c
$\widehat{\omega}_1 = (0,\, 2\pi) \times (\pi/2,\, 3\pi/2)$	0.3408	17	31.2907	0.0599	0.0019
$\widehat{\omega}_2 = (0,\, 2\pi) \times (\pi,\, 5.5991)$	0.3408	53	104.7046	0.0729	6.9624×10^{-4}
$\widehat{\omega}_3 = (0,\, 2\pi) \times (0,\, 1.6429)$	0.3408	154	139.1066	0.0709	5.0977×10^{-4}
$\widehat{\omega}_4 = (0,\, 2\pi) \times (\pi/2,\, \pi)$	0.1704	131	224.7782	0.0928	4.1291×10^{-4}
$\widehat{\omega}_5 = (0,\, 2\pi) \times (\pi,\, 3\pi/2)$	0.1704	131	224.7782	0.0928	4.1291×10^{-4}
$\widehat{\omega}_6 = (0,\, 2\pi) \times (0,\, 0.7354)$	0.1704	61	137.7779	0.0940	6.8238×10^{-4}

that for smooth surfaces of $\mathbb{R}^d$ (like the torus surface Σ considered in this article), the heat equation associated with the Laplace–Beltrami operator has the following property: $\forall\, T > 0$, and $y_0 \in \mathcal{L}^2(\Sigma)$, there exists $v \in \mathcal{L}^2(\omega \times (0,T))$, such that the corresponding solution of the heat equation verifies $y(T) = 0$. Among those controls realizing the null-controllability, one of particular interest is the unique control of minimal norm in $\mathcal{L}^2(\omega \times (0,\, T))$; the computation of this control has been discussed in [12] (a very inspiring article, indeed) for the heat equation on bounded domain of $\mathbb{R}^d$. Our goal, in this article is more modest: relying on Theorem 2.4 (with $y_{_T} = 0$), it is to use the penalty based methodology discussed in Sections 3 to 5, to compute an approximation of this control of minimal norm realizing the null–controllability, for values of k as large as possible.

Results with an smooth initial state

First, we investigate the above (approximate) null–controllability property with the initial smooth state y_0 defined on $\widehat{\Omega}$ by

$$y_0(\phi,\, \theta) = \cos\phi + \sin\theta. \tag{6.3}$$

We take, as before, $r = 1$, $R = 2$, the other parameters being also the same, namely $\mu = 2$, $\Delta t = 1/100$, $\Delta\phi = \Delta\theta = 2\pi/48$, $tol = 5 \times 10^{-5}$, $k = 10^8$, the conjugate gradient algorithm being initialized by $u_0 = 0$.

We began our numerical experiments with the supporting set $\widehat{\omega} = (0, 2\pi) \times (\pi/2, 3\pi/2)$, $k = 10^8$, and $T = 2$, 3 and 5. The numerical results reported in Table 12 show that for larger T the $\mathcal{L}^2$–norm of $y^c(T)$ gets smaller. Actually, this result is not surprising since in this particular case diffusion is not "fighting" against control, as it does in general, but "cooperate" with it in order to reach the null–state. In fact, in the absence of control (i.e., $u = 0$), the final state verifies: $||y^c_{nc}(T)||_{\mathcal{L}^2(\widehat{\Omega})}/||y_0||_{\mathcal{L}^2(\widehat{\Omega})} = 0.2562$, 0.1551 and 0.0570 if $T = 2$, 3 and 5, respectively, where y^c_{nc} is the computed non–controlled state function. This means that the reduction of (the norm of) the initial state by diffusion, after $T = 2$, 3 and 5 is about 74%, 84% and 94%, respectively.

We now study the behavior of null–controllability for horizontal supporting subdomains of different size. We chose $T = 3$ for these experiments. Table 13 shows that the computed state $y^c(T)$ gets closer to the null state as $|\omega|$ increases. The last two columns of this table show that: 1) the rate of decrease of $y^c(T)$ with respect to y_0, does not improve significantly

Table 9: Numerical results for $r/R \to 0$, with $R = 2$ fixed.

r	*No. Iters*	*Norm* u^c	*Rel. error*	$\|\omega\|$	$\omega\|/\|\Omega\|$
1	17	31.2907	0.0599	$4\pi(\pi-1)$	$(\pi-1)/2\pi = 0.3408$
1/2	17	20.8174	0.0681	$2\pi(\pi-1/2)$	$(\pi-1/2)/2\pi = 0.4204$
1/4	24	29.7111	0.0692	$\pi(\pi-1/4)$	$(\pi-1/4)/2\pi = 0.4602$
1/8	20	30.9316	0.0938	$(\pi/2)(\pi-1/8)$	$(\pi-1/8)/2\pi = 0.4801$
1/16	20	44.5047	0.1083	$(\pi/8)(\pi-1/16)$	$(\pi-1/16)/2\pi = 0.4901$

Table 10: Numerical results for $r/R \to 0$, with $r = 1$ fixed.

R	*No. Iters*	*Norm* u^c	*Rel. error*	$\|\omega\|$	$\omega\|/\|\Omega\|$
2	17	31.2907	0.0599	$4\pi(\pi-1)$	$(\pi-1)/2\pi = 0.3408$
4	11	37.4346	0.0639	$4\pi(2\pi-1)$	$(\pi-1/2)/2\pi = 0.4204$
8	11	50.3318	0.0591	$4\pi(4\pi-1)$	$(\pi-1/4)/2\pi = 0.4602$
16	9	69.0994	0.0590	$4\pi(8\pi-1)$	$(\pi-1/8)/2\pi = 0.4801$
32	9	96.4666	0.0577	$4\pi(16\pi-1)$	$(\pi-1/16)/2\pi = 0.4901$

when the size of the supporting set ω increases, except when $\omega = \Omega$; 2) the "real" rate of decrease, i.e. due to the application of control only (shown in last column), has a similar behavior. In fact, the quantities in the last column are equal to the quantities in the previous one multiplied by the constant $||y_0||/||y^c_{nc}(T)||$, which takes away the contribution of diffusion to the decrease of y_0 to the null state. We observe that the size of the supporting set for the control function does not play a significant role concerning the number of iterations necessary to achieve convergence. Figure 5 visualizes the evolution of the norm of the control for different values of k and the graph of the computed target $y^c(T)$. Of course, the small oscillations on the computed target are in the direction of θ, and more evident in between $\theta = \pi/2$ and $3\pi/2$, due to the horizontal subdomain employed to support the control.

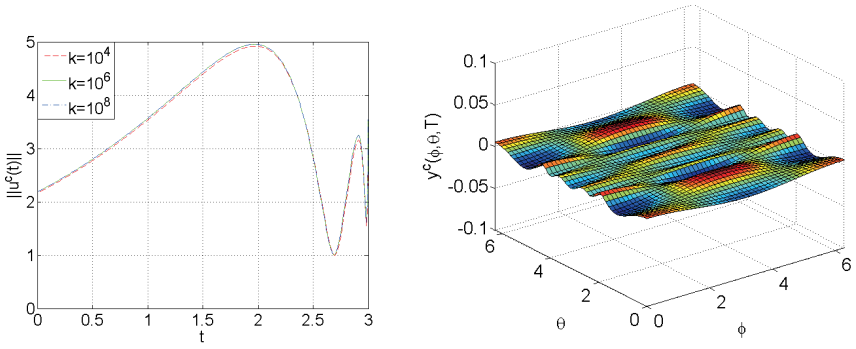

Figure 5: Left: Evolution of the norm of the computed control. Right: Graph of $y^c(T)$. Case for $\widehat{\omega} = (0, 2\pi) \times (2\pi/3, 4\pi/3)$ (null controllability).

Table 14 shows the numerical results with different vertical supporting subdomains. Again, the numerical results are not as good as those obtained with horizontal supporting subdomains.

Table 11: Numerical results for $r/R \to 0$, with $r = 1$ and $|\omega| = 4\pi(\pi - 1)$.

μ	R	$\widehat{\omega}$	$\lvert\omega\rvert/\lvert\Omega\rvert$	*No. Iters*	*Norm* u^c	*Rel. error*	*Rel. error/Norm* u^c
	2	$\widehat{\omega}_1$	0.3408	53	104.7046	0.0729	6.9624×10^{-4}
1/2	4	$\widehat{\omega}_2$	0.1704	141	139.1066	0.0709	3.0321×10^{-4}
	8	$\widehat{\omega}_3$	0.0852	66	417.4203	0.0900	2.1561×10^{-4}
	2	$\widehat{\omega}_1$	0.3408	36	66.6719	0.0671	0.0010
1	4	$\widehat{\omega}_2$	0.1704	39	115.0360	0.0859	7.4663×10^{-4}
	8	$\widehat{\omega}_3$	0.0852	37	169.9421	0.0858	5.0488×10^{-4}

Table 12: Dependence of null–controllability with respect to T. Case $\widehat{\omega} = (0, 2\pi) \times (\pi/2, 3\pi/2)$.

Quantity	$T = 2$	$T = 3$	$T = 5$
Number of iterations	13	14	11
Norm u^c	7.0289	3.9168	1.3460
$\lvert\lvert y^c(T)\rvert\rvert_{\mathcal{L}^2(\widehat{\Omega})}$	0.0412	0.0196	0.0118
$\lvert\lvert y^c(T)\rvert\rvert_{\mathcal{L}^2(\widehat{\Omega})}/\lvert\lvert y_0\rvert\rvert_{\mathcal{L}^2(\widehat{\Omega})}$	0.0046	0.0022	0.0013

Curves as supporting sets for null controllability

In the previous experiments we have seen that the numerical results for null controllability do depend on the size of the supporting set, $|\omega|$, but this dependence is marginal indeed. Thus, it suggests that we still may have good approximate null controllability properties if the control is supported by a horizontal coordinate curve γ of Σ and the initial state is the same smooth one defined in (6.3). The results presented in Table 15, obtained for $\gamma = \{\{\phi, \theta\} | 0 < \phi < 2\pi, \theta = \pi\}$, validate this prediction when $T = 2$, and 3.

In particular, the result with $T = 3$ compares favorably with those obtained when the horizontal supporting subdomains shown in Table 13 are employed; moreover, less conjugate gradient iterations are needed to achieve convergence.

Results with a non-smooth initial state

In order to investigate further the influence of the initial state, y_0, on the numerical results, we performed numerical experiments with the non–smooth initial state

$$y_0(\phi, \theta) = |\cos\phi| + |\sin\theta|,$$

which is a non–C^1 Lipschitz–continuous function of (ϕ, θ). Tables 16 and 17 summarize the numerical results: Table 16 is the analogue of Table 13 associated with the new function y_0. Similarly, Table 17 is the analogue of Table 15.

Table 13: Dependence of the approximate null–controllability with respect to $|\omega|$. Horizontal supporting subdomains.

$\widehat{\omega}$	$\lvert\omega\rvert/\lvert\Omega\rvert$	*No. iters*	*Norm* u^c	$\lvert\lvert y^c(T)\rvert\rvert_{\mathcal{L}^2(\widehat{\Omega})}$	$\frac{\lvert\lvert y^c(T)\rvert\rvert_{\mathcal{L}^2(\widehat{\Omega})}}{\lvert\lvert y_0\rvert\rvert_{\mathcal{L}^2(\widehat{\Omega})}}$	$\frac{\lvert\lvert y^c(T)\rvert\rvert_{\mathcal{L}^2(\widehat{\Omega})}}{\lvert\lvert y^c_{nc}(T)\rvert\rvert_{\mathcal{L}^2(\widehat{\Omega})}}$
$(0,2\pi)\times(0,2\pi)$	1	2	1.4188	2.0748×10^{-5}	2.3383×10^{-6}	1.5078×10^{-5}
$(0,2\pi)\times(\pi/2,3\pi/2)$	0.3408	14	3.9167	0.0196	0.0022	0.0142
$(0,2\pi)\times(2\pi/3,4\pi/3)$	0.1955	15	6.2900	0.0290	0.0033	0.0211
$(0,2\pi)\times(3\pi/4,5\pi/4)$	0.1375	14	7.9594	0.0412	0.0046	0.0299
$(0,2\pi)\times(7\pi/8,9\pi/8)$	0.0641	24	11.7634	0.0489	0.0055	0.0355
$(0,2\pi)\times(15\pi/16,17\pi/16)$	0.0320	19	14.7410	0.0556	0.0063	0.0404

Table 14: Dependence of null–controllability with respect to $|\omega|$. Vertical supporting subdomains.

$\phi_f-\phi_0$	$\lvert\omega\rvert/\lvert\Omega\rvert$	*No. iters*	*Norm* u^c	$\lvert\lvert y^c(T)\rvert\rvert_{\mathcal{L}^2(\widehat{\Omega})}$	$\frac{\lvert\lvert y^c(T)\rvert\rvert_{\mathcal{L}^2(\widehat{\Omega})}}{\lvert\lvert y_0\rvert\rvert_{\mathcal{L}^2(\widehat{\Omega})}}$	$\frac{\lvert\lvert y^c(T)\rvert\rvert_{\mathcal{L}^2(\widehat{\Omega})}}{\lvert\lvert y^c_{nc}(T)\rvert\rvert_{\mathcal{L}^2(\widehat{\Omega})}}$
π	0.5000	26	5.4407	0.0911	0.0103	0.0662
$2\pi/3$	0.3333	41	10.4483	0.1039	0.0117	0.0755
$\pi/2$	0.2500	38	13.1074	0.1569	0.0177	0.1140
$\pi/4$	0.1250	49	23.3285	0.1608	0.0181	0.1169

Table 15: Approximate null controllability. Case of the horizontal line $\theta=\pi$.

T	*No. iters*	*Norm* u^c	$\lvert\lvert y^c(T)\rvert\rvert_{\mathcal{L}^2(\widehat{\Omega})}$	$\frac{\lvert\lvert y^c(T)\rvert\rvert_{\mathcal{L}^2(\widehat{\Omega})}}{\lvert\lvert y_0\rvert\rvert_{\mathcal{L}^2(\widehat{\Omega})}}$	$\frac{\lvert\lvert y^c(T)\rvert\rvert_{\mathcal{L}^2(\widehat{\Omega})}}{\lvert\lvert y^c_{nc}(T)\rvert\rvert_{\mathcal{L}^2(\widehat{\Omega})}}$
2	8	198.8242	0.1386	0.0156	0.0610
3	7	105.4722	0.0296	0.0033	0.0215

Table 16: Dependence with respect to $|\omega|$ of the approximate null–controllability with a non-smooth initial state.

$\widehat{\omega}$	$\lvert\omega\rvert/\lvert\Omega\rvert$	*No. iters*	*Norm* u^c	$\lvert\lvert y^c(T)\rvert\rvert_{\mathcal{L}^2(\widehat{\Omega})}$	$\frac{\lvert\lvert y^c(T)\rvert\rvert_{\mathcal{L}^2(\widehat{\Omega})}}{\lvert\lvert y_0\rvert\rvert_{\mathcal{L}^2(\widehat{\Omega})}}$	$\frac{\lvert\lvert y^c(T)\rvert\rvert_{\mathcal{L}^2(\widehat{\Omega})}}{\lvert\lvert y^c_{nc}(T)\rvert\rvert_{\mathcal{L}^2(\widehat{\Omega})}}$
$(0,2\pi)\times(\pi/2,3\pi/2)$	0.3408	10	12.5523	0.0812	0.0068	0.0072
$(0,2\pi)\times(2\pi/3,4\pi/3)$	0.1955	9	17.2856	0.1033	0.0087	0.0092
$(0,2\pi)\times(3\pi/4,5\pi/4)$	0.1375	10	20.7466	0.1062	0.0089	0.0094
$(0,2\pi)\times(7\pi/8,9\pi/8)$	0.0641	14	29.3117	0.1100	0.0092	0.0098
$(0,2\pi)\times(15\pi/16,17\pi/16)$	0.0320	9	36.1717	0.1175	0.0098	0.0104

Table 17: Approximate null controllability. Case of the horizontal line $\theta=\pi$ (for a non-smooth initial state).

T	*No. iters*	*Norm* u^c	$\lvert\lvert y^c(T)\rvert\rvert_{\mathcal{L}^2(\widehat{\Omega})}$	$\frac{\lvert\lvert y^c(T)\rvert\rvert_{\mathcal{L}^2(\widehat{\Omega})}}{\lvert\lvert y_0\rvert\rvert_{\mathcal{L}^2(\widehat{\Omega})}}$	$\frac{\lvert\lvert y^c(T)\rvert\rvert_{\mathcal{L}^2(\widehat{\Omega})}}{\lvert\lvert y^c_{nc}(T)\rvert\rvert_{\mathcal{L}^2(\widehat{\Omega})}}$
2	5	335.2381	0.2936	0.0246	0.0261
3	5	234.2418	0.1427	0.0120	0.0127

Comparing Tables 13 and 15 to Tables 16 and 17 shows that the initial smooth state $y_0(\phi,\,\theta)=\cos\phi+\sin\theta$ leads to better approximate null–controllability results than $y_0(\phi,\,\theta)=|\cos\phi|+|\sin\theta|$. The significant difference we observe does not stem from the (relative)

non–smoothness of the second initial state, but from the fact that it verifies $\int_\Sigma y_0\, d\Sigma \neq 0$. Indeed, left uncontrolled, the solution of the state equation will verify $\lim_{t\to+\infty} y(t) = (1/|\Sigma|)\int_\Sigma y_0\, d\Sigma \neq 0$, where $|\Sigma|$ = measure of Σ. Cancelling (or nearly cancelling) the contribution of the constant component of the solution is what makes the calculation of the control more costly in this case. However, even in this more difficult situation, our methodology does not behave badly, as shown by the last two columns of Tables 16 and 17. In Figure 6 we show the evolution of the norm of the control and the graph of the computed target $y^c(T)$, for the case in which the supporting set for the control is $\widehat{\omega} = (0, 2\pi) \times (2\pi/3, 4\pi/3)$.

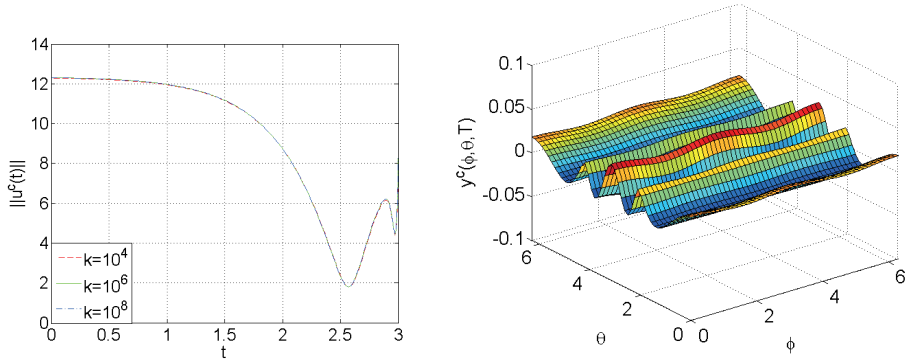

Figure 6: Left: evolution of the norm of the computed control. Right: graph of $y^c(T)$. Null controllability with non-smooth y_0 and supporting set $\widehat{\omega} = (0, 2\pi) \times (2\pi/3, 4\pi/3)$.

As a final numerical experiment, let us consider the (still) non–smooth initial state

$$y_0 = |\cos\phi| + |\sin\theta| - \frac{4}{\pi}, \tag{6.4}$$

which satisfy $\bar{y}_0 = (1/|\Sigma|)\int_{\widehat{\Omega}} y_0\, d\Sigma = 0$. In this case we obtain much better controllability results as shown in Table 18 and in Figure 7, showing that the employed numerical methodology solves the null–controllability problem in a satisfactory way at least with this y_0 (although more conjugate gradient iterations are needed to achieve convergence).

Table 18: Approximate null controllability. Case of the horizontal line $\theta = \pi$ (for a non–smooth initial state with $\bar{y}_0 = 0$).

T	*No. iters*	*Norm* u^c	$\|\|y^c(T)\|\|_{\mathcal{L}^2(\widehat{\Omega})}$	$\frac{\|\|y^c(T)\|\|_{\mathcal{L}^2(\widehat{\Omega})}}{\|\|y_0\|\|_{\mathcal{L}^2(\widehat{\Omega})}}$	$\frac{\|\|y^c(T)\|\|_{\mathcal{L}^2(\widehat{\Omega})}}{\|\|y^c_{nc}(T)\|\|_{\mathcal{L}^2(\widehat{\Omega})}}$
2	49	66.6718	0.0043	0.0011	0.0411
3	21	11.2341	0.0029	7.4238×10^{-4}	0.0862

7 Comments and Conclusions

In this article, we have investigated the numerical solution of approximate controllability problems for a diffusion process taking place on the surface Σ of a torus. Two types of control problems have been investigated: (i) Problems associated with *non–zero* target functions

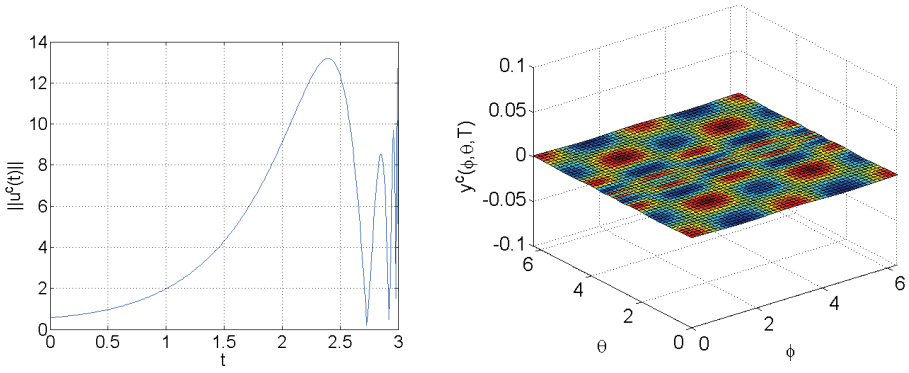

Figure 7: Left: evolution of the norm of the computed control. Right: graph of $y^c(T)$. Null controllability with non–smooth y_0 (where $\bar{y}_0 = 0$) and supporting set $\theta = \pi$.

y_T. (ii) Null–controllability problems, leading to results consistent with those proved in [9]. Concerning the problem of finding the control of minimal norm realizing null–controllability let us mention that it can be formulated as

$$\Lambda u = f \tag{7.1}$$

where

(i) Λ is a positive self–adjoint injective compact linear (pseudo–differential) operator from $\mathscr{U}$ $(= \mathcal{L}^2(\omega \times (0, T)))$ into itself.

(ii) f is a linear function of the initial data y_0.

Problem (7.1) is a kind of elliptic problem, however, since Λ is not an isomorphism of $\mathscr{U}$, solving problem (7.1) numerically is a non–trivial issue (reminiscent of the difficulties one encounters when solving numerically Fredholm integral equations of the first kind). The numerical solution of problems like (7.1), associated with the heat equation in bounded domains of $\mathbb{R}^d$, has been successfully addressed in [3], [4], [11], [12]. The simple (but robust) penalty based procedure we advocate in this article is equivalent to approximating (7.1) by

$$k^{-1}u + \Lambda u = f, \tag{7.2}$$

a typical *Tychonoff regularization procedure* indeed (the operator $k^{-1}I + \Lambda$ is a self–adjoint strongly elliptic isomorphism of $\mathscr{U}$, making problem (7.2) well–posed and its solution by a conjugate gradient algorithm operating in $\mathscr{U}$ possible).

The methodology discussed in this article applies also to other surfaces of $\mathbb{R}^3$, such as spheres, a topic we are currently investigating; actually the preliminary numerical results we have obtained for spheres look very promising and, not surprisingly, are consistent with those reported in this article.

Acknowledgments

The authors want to acknowledge the financial support from CONACYT (National Council of Science and Technology in Mexico) through a scholarship for the first author, who did

an one year internship at the University of Houston under the supervision of the second author. We acknowledge also the support from the Math Graduate program at Universidad Aut坦noma Metropolitana, and from the Institute for Advanced Studies at the Hong Kong University of Sciences and Technology. Finally, special thanks are due to the anonymous referees for their valuable advices and suggestions.

References

[1] A. Bonito and R. Glowinski, On the nodal set of the eigenfunctions of the Laplace–Beltrami operator for bounded surfaces in $\mathbb{R}^3$; A computational approach, *Commun. Pure Appl. Anal.* **13** (2014) 2115–2126.

[2] C. Carthel, R. Glowinski and J.L. Lions, On exact and approximate boundary controllabilities for the heat equation: A numerical approach, *J. Optim. Theory Appl.* **82**(1994) 429–484.

[3] E. Fernández–Cara and A. Münch, Strong convergent approximations of null controls for the 1D heat equation, SEMA Journal **61** (2013) 49–78.

[4] E. Fernández–Cara and A. Münch, Numerical null controllability of the 1D heat equation: Duality and Carleman weights, *J. Optim. Theory Appl.* **163** (2014) 253–285.

[5] R. Glowinski, *Numerical Methods for Nonlinear Variational Problems*, Springer, New York, 1984 (2^{nd} printing: 2008).

[6] R. Glowinski, Finite element methods for incompressible viscous flow, in *Handbook of Numerical Analysis*, **Vol. IX**, P.G. Ciarlet and J.L. Lions, eds., North-Holland, Amsterdam, 2003, pp. 3-1176.

[7] R. Glowinski, J.L. Lions and J.W. He, *Exact and Approximate Controllability for Distributed Parameter Systems: A Numerical Approach*, Cambridge University Press, Cambridge, UK, 2008.

[8] R. Glowinski and D.C. Sorensen, Computing the eigenvalues of the Laplace-Beltrami operator on the surface of a torus: A numerical approach, in *Partial Differential Equations: Modelling and Numerical Simulation*, R. Glowinski & P.Neittaanmäki, eds., Springer Netherlands, (2008), 225–232.

[9] G. Lebeau and L. Robbiano, Contrôle exact de l'équation de la chaleur, *Comm. Partial Differential Equations* **20** (1995) 335–356.

[10] J.L. Lions, *Optimal Control of Systems Governed by Partial Differential Equations*, Springer-Verlag, New York, 1971.

[11] A. Münch and P. Pedregal, Numerical null controllability of the heat equation through a least squares and variational approach, *European J. Appl. Math.* **25** (2014) 277–306.

[12] A. Münch and E. Zuazua, Numerical approximation of null controls for the heat equation: Ill-posedness and remedies, Inverse Problems, **26** (2010) 085018, 39.

Manuscript received 20 January 2015
revised 26 February 2015
accepted for publication 26 February 2015

D. Assaely León-Velasco
Departamento de Matemáticas
Universidad Autónoma Metropolitana Unidad Iztapalapa
Av. San Rafael Atlixco 186, Col. Vicentina, D.F. 09340, Mexico
E-mail address: assaely@xanum.uam.mx

Roland Glowinski
Deparment of Mathematics, University of Houston
4800 Calhoun, Houston, TX 77004, USA, and
Baptist University, Hong-Kong.
E-mail address: roland@math.uh.edu

L. Héctor Juárez-Valencia
Departamento de Matemáticas
Universidad Autónoma Metropolitana Unidad Iztapalapa
Av. San Rafael Atlixco 186, Col. Vicentina, D.F. 09340, Mexico
E-mail address: hect@xanum.uam.mx